Numerical Heat Transfer, Part A: Applications: An International Journal of Computation and Methodology

PROPAGATION AND REFLECTION OF THERMAL WAVES IN A RECTANGULAR PLATE

Jhy-Ping Wu, Hsin-Sen Chu
Published online: 29 Oct 2010.

PLEASE SCROLL DOWN FOR ARTICLE

PROPAGATION AND REFLECTION OF THERMAL WAVES IN A RECTANGULAR PLATE

Jhy-Ping Wu and Hsin-Sen Chu
Department of Mechanical Engineering, National Chiao Tung University,
Hsinchu, Taiwan 300, Republic of China

The wave nature of heat propagation in a two-dimensional rectangular plate with an instantaneous thermal disturbance released in an arbitrary position is investigated by solving the hyperbolic heat conduction equation. The exact analytical solutions are developed for the temperature field and heat flux using the Green's function technique to deal with two limiting boundary conditions, the constant wall temperature and the adiabatic condition, around the region. The disturbance gives rise to a severe thermal wave front, which differs completely from that obtained through one-dimensional analysis, traveling through the medium at a finite speed with a sharp peak at the leading edge. The significant findings in these results are that a negative trailer is generated and follows behind the wave front. In addition, the magnitude of the front is significantly attenuated from the side adjacent to the trailer because the increasing area available to it for diffusion, and decays exponentially along its path of travel, since the thermal energy is dissipated in the wake of the moving wave front. The results also reveal that different boundary conditions strongly influence the reflection of a thermal wave front from the exterior surfaces and the reflection and interaction among thermal waves are more complicated than those found through one-dimensional analysis.

INTRODUCTION

The Fourier law of heat conduction, which is the classical theory of diffusion, postulates a heat flux to be directly proportional to a temperature gradient in the form

$$q(r, t) = -k \nabla T(r, t) \tag{1}$$

where k is the thermal conductivity, r the position vector, and t the physical time. According to this law, the traditional heat conduction equation implies an infinite speed of propagation of the thermal wave, indicating that a local change in temperature causes an instantaneous perturbation in the temperature at each point in the medium, even if the intervening distances are infinitely large. In other words, heat propagates infinitely fast, which is incompatible with physical reality. Despite such an illogical notion of energy transport in solids, the classical diffusion

NOMENCLATURE

a, b	plate lengths in the x and y directions	(X_0, Y_0)	dimensionless position of heat source
A, B	dimensionless plate lengths in the X and Y directions	α	thermal diffusivity
		δ	Dirac delta function
c	thermal wave speed	$\Delta x, \Delta y$	thermal disturbance widths in x and y directions, respectively
C_p	specific heat		
g	volumetric energy source	$\Delta X, \Delta Y$	dimensionless thermal disturbance widths in x and y directions, respectivly
g_0	total energy released per unit length, as defined by Eq. (7)		
$G(X, Y,$	Green's function	θ	dimensionless temperature
$\tau \mid \xi, \eta, \zeta)$		Φ_{mn}	finite integral transform operator
$\hat{G}_{mn}(\tau)$	transform of Green's function	λ_{mn}	eigenvalue
H	Heaviside function	ξ, η, ζ	dummy variables replacing dimensionless variables X, Y, and τ, respectively, in Green's function technique
k	thermal conductivity		
q	heat flux		
Q	dimensionless heat flux	ρ	density
r	position vector	τ	dimensionless time
S	dimensionless energy source	τ_R	relaxation time
t	time		
T	temperature	**Subscripts**	
$\mathbf{T}$	arbitrary number (> 0)	m, n	indices
T_0	initial temperature	x, y	components in x and y direction, respectively
x, y	Cartesian coordinate		
X, Y	dimensionless Cartesian coordinate	X, Y	components in X and Y direction, respectively
(x_0, y_0)	position of heat source		

theory has been widely applied in heat transfer problems and gives reliable results for most situations encountered in practice, mainly because in most situations the thermal diffusivity is 10 orders of magnitude smaller than that corresponding to the speed of a thermal wave. However, with the advent of science and technology dealing with very low temperatures near absolute zero, an extremely short transient duration, and an extremely high rate change of temperature or heat flux, some investigators have found that the heat propagation velocity in such situations becomes finite and dominant.

One of the earliest experiments aimed at detecting thermal waves was performed by Peshkov [1] using superfluid liquid helium at a temperature of 1.4 K and having a thermal wave velocity of 19 m/s. He referred to this phenomenon as "second sound" because of the similarity between thermal waves he observed and ordinary acoustic waves. Von Gutfeld [2] measured that the velocities of thermal waves in different dielectric crystals, such as sapphire, GeSi, and NaCl, are all of the order of 10^3 m/s at low temperatures. Maurer and Thompson [3] found that if the surface heat fluxes are of an order greater than 10^7 W/m^2, the Fourier heat flux model breaks down.

In recent years, because of advancements in short-pulse laser technologies and their applications to modern microfabrication technologies, research of high-rate heating on thin film structures has progressed rapidly. To consider the finite speed of wave propagation, a damped-wave model has been proposed that uses a

variety of reasonings and derivations. Its development is presented in detail in the exhaustive review articles by Joseph and Preziosi [4, 5]. Cattaneo [6] and Vernotte [7] independently suggested a modified heat flux model of the form

$$q(r, t + \tau_R) = -k\,\nabla T(r, t) \tag{2}$$

where τ_R is relaxation time, an intrinsic thermal property of media. Equation (2) implies that the temperature gradient established at time t, due to insufficient response time, results in a heat flux vector at a later time $t + \tau_R$. This means the heat wave model allows a time lag between the heat flux and the temperature gradient. In fact, the relaxation time τ_R is associated with the communication "time" between phonons (phonon-phonon collisions) necessary for commencement of heat flow and is a measure of the thermal inertia of a medium. Based on ideas from the collision theory of molecules, $\tau_R \approx \alpha/c^2$, where c is the thermal wave velocity in the medium. Clearly, for $\tau_R = 0$, Eq. (2) reduces to the classical Fourier's law and leads to an infinite propagation velocity. Several investigators attempted to estimate the magnitude of τ_R for common engineering materials [8, 9]. It appears that the magnitude of τ_R ranges from 10^{-10} s for gases under standard conditions to 10^{-14} s for metals, with values of τ_R for liquids and insulators falling within this range. Sieniutycz [10] showed that the τ_R values for a homogeneous substance are of the order of 10^{-8}–10^{-10} s, while recent work by Kaminsky [11] on nonhomogeneous inner structure materials revealed values for τ_R of the order of fractions of a minute. Recently, Mitra et al. [12] determined experimentally that the value of τ_R is $\sim$ 16 s for biological materials, and directly validated the hyperbolic nature of heat conduction by comparing experimentally observed temperatures with corresponding non-Fourier predictions.

To emphasize engineering applications of the thermal wave theory, Özisik and Tzou [13] presented a thorough review of thermal wave propagation that included a sharp wave front and rate effects, the thermal shock phenomenon, thermal resonance phenomenon, and reflections and refractions of thermal waves across a material interface. They also employed the concept of dual phase lag to capture the microscopic mechanisms in some limiting cases. A general criterion for the dominance of wave behavior over diffusion was proposed by Tzou [14]:

$$\frac{\partial T}{\partial t} \gg \left[\frac{T_0 c^2}{2\alpha} \exp\left(\frac{c^2 t}{\alpha}\right) \right] \tag{3}$$

T_0 being the reference temperature. According to this criterion, the relative importance of the wave behavior in heat conduction can be examined by considering the interaction of three factors, the thermal properties (α and c), the thermal loading and response conditions ($\partial T/\partial t$, and T_0), and the transient time (t). If the heat transfer process occurs in an extremely short period of time or at an extremely high rate of temperature increase, the wave behavior may become pronounced regardless of the value of T_0.

Various analytical and numerical methods were proposed to solve hyperbolic heat conduction problems [15–19]. Analytical solutions were developed by Özisik

and Vick [20] for the hyperbolic heat conduction equation in a one-dimensional finite slab with insulated boundaries subjected to a volumetric energy source in the medium specifically to explore the propagation and reflection of thermal waves in a finite medium. Recently, Haji-Sheikh and Beck [21] presented a general form of the Green's function solution method for a wave-type conduction equation in a finite body and employed a convergence-accelerating technique when using a series solution to describe an abrupt change in temperature. However, most problems involving complicated geometries and conditions or variable physical properties are difficult to solve analytically, and numerical solutions must be sought. To the best of the authors' knowledge, only a few researchers have focused attention on the thermal wave behavior caused by a single thermal disturbance in multidimensional geometry. Recently, Wu et al. [22] presented a numerical analysis of the two-dimensional hyperbolic heat conduction problem in an anisotropic medium under a point heat source with different boundary conditions. They found that the transient behavior of the propagation of the two-dimensional thermal wave is much more complicated than that of the one-dimensional thermal wave because of the reflections by boundaries and interactions with each other.

Recently, Tamma and Namburu [23] pointed out that interdisciplinary problems encompassing thermal sciences and structural mechanics/dynamics disciplines are encountered in a number of applications in mechanical, aerospace, and nuclear engineering. Thermomechanical interactions in materials and structures are an important consideration in the design/analysis of mechanical components. A unified computational methodology and algorithmic representation for nonclassical/classical thermomechanical problems relevant to thermal stress wave propagation, thermally induced structural dynamics, and thermal stress problems was described with applications to various illustrative examples. More recently, Tamma and Zhou [24] also presented some noteworthy perspectives of macroscale and microscale thermal transport including thermomechanical interactions in materials and structures.

This investigation was concerned with the propagation of a thermal wave in a rectangular plate with an initial thermal disturbance located in an arbitrary position. The effects of thermomechanical interactions are ignored. Two kinds of boundary conditions, a constant wall temperature (that is, a continuous, constant temperature equivalent to the initial temperature) and an adiabatic condition, were considered, and the boundary conditions on four exterior sides were assumed to be the same. We use the Green's function technique to solve the above boundary value problem. The results showed that the disturbance induces a severe thermal wave front that traverses the medium with a sharp peak at the leading edge and generates a negative trailer that follows behind the wave front. Moreover, the reflection and interaction of thermal waves are complicated by two factors, the finite area of the thermal disturbance and the boundary conditions. These results are strikingly different from those for a one-dimensional analysis.

ANALYSIS

By applying Taylor's series expansion to q in Eq. (2) with respect to τ_R, and then neglecting the second- and higher-order terms of τ_R, the Maxwell-Cattaneo

equation or non-Fourier's law can be obtained:

$$q(r, t) + \tau_R \frac{\partial q(r, t)}{\partial t} = -k \nabla T(r, t) \qquad (4)$$

Equation (4) is the constitutive equation used in the linearized thermal wave theory. The elimination of heat flux q between Eq. (4) and the energy conservation equation leads to the following hyperbolic heat conduction equation with energy sources for the temperature distribution:

$$\frac{1}{c^2} \frac{\partial^2 T}{\partial t^2} + \frac{1}{\alpha} \frac{\partial T}{\partial t} = \nabla^2 T + \frac{1}{k} \left(g + \frac{\alpha}{c^2} \frac{\partial g}{\partial t} \right) \qquad (5)$$

where g represents the volumetric energy source in the medium and $\alpha = k/\rho C_p$. The thermal properties and the thermal relaxation time are assumed to be constant. For the case in which $c \to \infty$, Eq. (5) reduces to the classical heat diffusion equation, which corresponds to instantaneous energy diffusion.

In this investigation a two-dimensional heat conduction problem in a rectangular plane with constant thermal properties was considered. The thermal conductivity and the velocity of a thermal wave were assumed to be isotropic in the medium. The region was initially in equilibrium at temperature T_0. The boundary conditions of the four sides were the same, and two kinds of boundary conditions, the adiabatic and a constant wall temperature equal to the initial one, were considered. The geometry and Cartesian coordinates are depicted in Figure 1. The internal heat source initiated by some distributed energy source, $g(x, y, t)$, is located at an arbitrary location (x_0, y_0) when times $t > 0$. The widths of the plane in the x and y directions are a and b, respectively.
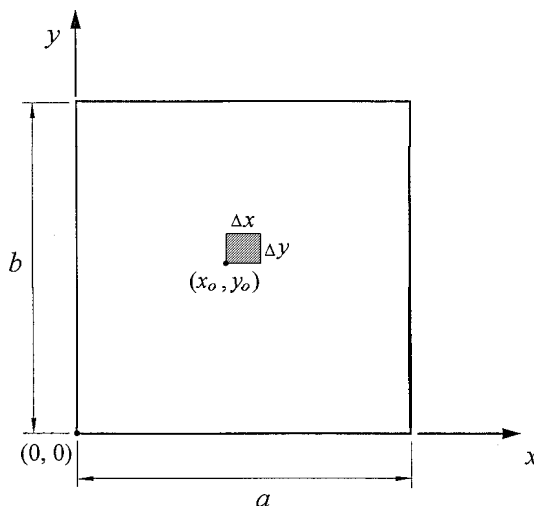

Figure 1. Schematic drawing of the physical model.

For convenience in the subsequent analysis, the nondimensionalized variables are defined in the transformed system as follows:

$$X = \frac{cx}{2\alpha} \qquad Y = \frac{cy}{2\alpha} \qquad \tau = \frac{c^2 t}{2\alpha} \tag{6a}$$

$$\theta(X, Y, \tau) = \frac{T(x, y, t) - T_0}{g_0 c/k} \qquad Q_X(X, Y, \tau) = \frac{q_x(x, y, t)}{g_0 c^2/\alpha} \tag{6b}$$

$$Q_Y(X, Y, \tau) = \frac{q_y(x, y, t)}{g_0 c^2/\alpha} \qquad S(X, Y, \tau) = \frac{g(x, y, t)}{g_0 c^4/8\alpha^3} \tag{6c}$$

where the reference quantity g_0 is considered to be finite and is defined as

$$g_0 = \int_{t=0}^{\infty} \int_{x=0}^{a} \int_{y=0}^{b} g(x, y, t) \, dy \, dx \, dt \tag{7}$$

which represents the total energy released per unit length normal to the xy plane over the entire region over all times.

The energy equation and its initial conditions are expressed in terms of the above dimensionless variables as

$$\frac{\partial^2 \theta}{\partial \tau^2} + 2\frac{\partial \theta}{\partial \tau} = \frac{\partial^2 \theta}{\partial X^2} + \frac{\partial^2 \theta}{\partial Y^2} + \left(S + \frac{1}{2}\frac{\partial S}{\partial \tau} \right) \tag{8}$$
$$0 < X < A \qquad 0 < Y < B \qquad \tau > 0$$

where $A = ca/2a$, $B = cb/2a$. Initial conditions are

$$\theta(X, Y, \tau = 0) = \frac{\partial \theta}{\partial \tau}(X, Y, \tau = 0) = 0 \tag{9}$$

To understand the different boundary conditions influencing the propagation and reflection of the heat wave, two limiting boundary cases were selected for consideration. One is the prescribed temperature at which the temperature at the boundaries was equal to T_0. This means the heat transfer coefficient of the surroundings approaches infinity. Conversely, the other case was an adiabatic boundary condition under which no heat flux is transferred through the boundary. Therefore the heat was fully reflected by the boundaries and restricted within the medium. The foregoing governing equation, Eq. (8), was thus considered subject to the two kinds of boundary conditions mentioned above and is summarized below.

Constant wall temperature

$$\theta(X = 0, Y, \tau) = 0 \qquad 0(X = A, Y, \tau) = 0 \tag{10a}$$

$$\theta(X, Y = 0, \tau) = 0 \qquad 0(X, Y = B, \tau) = 0 \tag{10b}$$

Adiabatic

$$\frac{\partial \theta}{\partial X}(X= 0, Y, \tau) = 0 \qquad \frac{\partial \theta}{\partial X}(X= A, Y, \tau) = 0 \tag{11a}$$

$$\frac{\partial \theta}{\partial Y}(X, Y= 0, \tau) = 0 \qquad \frac{\partial \theta}{\partial Y}(X, Y= B, \tau) = 0 \tag{11b}$$

The Green's function solution method is a good and simple procedure for obtaining a solution to the heat wave equation [21]. First, the problem with regard to the governing system of equations, Eqs. (8)–(11), was subjected to arbitrary dimensionless heat generation, $S(X, Y, \tau)$. The analytical solution of the system is expressed in terms of a Green's function of the form [25]

$$\theta(X, Y, \tau) = \int_{\xi=0}^{A} \int_{\eta=0}^{B} \int_{\zeta=0}^{\tau} G(X, Y, \tau|\xi, \eta, \zeta) \cdot \left(S(\xi, \eta, \zeta) + \frac{1}{2}\frac{\partial S}{\partial \zeta}\right) d\zeta\, d\eta\, d\xi \tag{12}$$

Here the Green's function, $G(X, Y, \tau|\xi, \eta, \zeta)$, represents the fundamental solution of the problem governed by Eqs. (8)–(11) with the arbitrary nonhomogeneous contribution, $S(\xi, \eta, \zeta) + 1/2(\partial S/\partial \zeta)$, replaced by a quantity of heat released at point (ξ, η) at time ζ according to the unit-impulse function $\delta(X- \xi)\delta(Y- \eta)\delta(\tau- \zeta)$. The $\delta(x)$ represents the Dirac delta function. Once the Green's function is found, the temperature distribution can be solved by Eq. (12). Therefore the key ingredient in this analytical development is to determine the Green's function, the definition of which presented here is different from that given by Haji-Sheikh and Beck [21]. They showed that a solution of the Fourier-type diffusion equation serves as a building block in constructing a solution for the heat wave equation.

The Green's function satisfies the following governing equation:

$$\frac{\partial^2 G}{\partial \tau^2} - 2\frac{\partial G}{\partial \tau} = \frac{\partial^2 G}{\partial X^2} + \frac{\partial^2 G}{\partial Y^2} + \delta(X- \xi)\delta(Y- \eta)\delta(\tau- \zeta) \tag{13}$$
$$0 < X < A \qquad 0 < Y < B \qquad \tau, \zeta < \mathbf{T}$$

In addition, $G(X, Y, \tau|\xi, \eta, \zeta)$ satisfies the initial conditions or, equivalently, the end conditions,

$$G(X, Y, \mathbf{T}|\xi, \eta, \zeta) = \frac{\partial G}{\partial \tau}(X, Y, \mathbf{T}|\xi, \eta, \zeta) = 0 \tag{14}$$

and the boundary conditions,

$$pG + q\frac{\partial G}{\partial X} = 0 \qquad X= 0 \text{ or } A, \tau, \zeta < \mathbf{T} \tag{15}$$

$$pG + q\frac{\partial G}{\partial Y} = 0 \qquad Y= 0 \text{ or } B, \tau, \zeta < \mathbf{T} \tag{16}$$

The initial conditions, Eq. (14), are based on the causality principle, which states that an effect cannot be experienced at any time prior to its cause, whereas the boundary conditions, Eqs. (15) and (16), depend on different combinations of the coefficients p and q. If a constant wall temperature at the boundaries is specified, then $p = 1$ and $q = 0$ are required. On the other hand, if an adiabatic boundary condition is given, the coefficients must be $p = 0$ and $q = 1$.

The multiple finite transform technique [26] for two independent variables X and Y is used to solve the two-dimensional system Eqs. (13)–(16). Using this transform, an ordinary differential equation and initial conditions with respect to time, τ, can be obtained. Then we can obtain the Green's function using a straightforward series of manipulations along with the inversion theorem as follows:

$$G(X, Y, \tau \mid \xi, \eta, \zeta) = e^{-(\tau - \zeta)} H(\tau - \zeta)$$

$$\times \sum_{m=0}^{\infty} \sum_{n=0}^{\infty} \frac{\sin\left[(\tau - \zeta)\sqrt{\lambda_{mn} - 1}\right]}{\sqrt{\lambda_{mn} - 1}} \frac{\Phi_{mn}(\xi, \eta)\Phi_{mn}(X, Y)}{(\Phi_{mn}, \Phi_{mn})}$$

$$(17)$$

where λ_{mn} are the allowable eigenvalues, Φ_{mn} is the operator of finite integral transform, and $H(t)$ is the Heaviside function. Next, this fundamental solution is then introduced into Eq. (12) to obtain the temperature distribution as

$$\theta(X, Y, \tau) = \int_{\xi=0}^{A} \int_{\eta=0}^{B} \int_{\zeta=0}^{\tau} e^{-(\tau - \zeta)}$$

$$\times \sum_{m=0}^{\infty} \sum_{n=0}^{\infty} \frac{\sin\left[(\tau - \zeta)\sqrt{\lambda_{mn} - 1}\right]}{\sqrt{\lambda_{mn} - 1}} \frac{\Phi_{mn}(\xi, \eta)\Phi_{mn}(X, Y)}{(\Phi_{mn}, \Phi_{mn})}$$

$$\times \left(S(\xi, \eta, \zeta) + \frac{1}{2}\frac{\partial S}{\partial \zeta}\right) d\zeta \, d\eta \, d\xi \qquad (18)$$

where the heat generation S can be given in many forms. The Heaviside function $H(\tau - \zeta)$ in Eq. (17) vanishes and is transformed into an integral with respect to time, ζ, from 0 to τ.

The fundamental nature of hyperbolic heat conduction is best represented by considering a thermal disturbance deposited in a volumetric source of area $\Delta x \Delta y$. The energy is located in an arbitrary position (x_0, y_0) and released instantaneously at time $t = 0$ with a total strength or energy content per unit length normal to the xy plane of g_0. Such an energy source could serve as a model, for example, application of film/tape superconductors, which is associated with thermal stability under thermal disturbances caused by a sudden relaxation of dislocations, crystal defects, or other spontaneous processes in superconductors [27]. This situation assumes both the film/tape and the disturbance source to be infinite lengths along the current direction, and Figure 1 displays the profile of a cross section normal to

the current direction. Another important application concerns a strong or ultra-short-duration laser beam irradiation of absorbing or thin media surfaces. If the absorbent layer is sufficiently comparable with the thickness of the medium, the energy pulse may be assumed a volumetric source of finite area. Therefore this physical model can be considered to lump the system in the thickness variable if the upper and lower surfaces of the plane are also assumed to be adiabatic. In this example, Figure 1 shows the upper surface of the plane. Such energy sources can be described mathematically as

$$g(x, y, \tau) = \begin{cases} \dfrac{g_0 \delta(t)}{\Delta x \Delta y} & x_0 \leqslant x \leqslant x_0 + \Delta x \qquad y_0 \leqslant y \leqslant y_0 + \Delta y \\ 0 & \text{otherwise} \end{cases} \qquad (19)$$

where g_0 is given in Eq. (7) and $\delta(t)$ is the Dirac delta function. Here the delta function with respect to time means the limit of a pulse-type function as the pulse becomes infinitely concentrated. By introducing the dimensionless quantities Eqs. $(6a)$–$(6c)$, the corresponding dimensionless form of the heat generation function, Eq. (19), can be expressed as

$$S(X, Y, \tau) = \begin{cases} \dfrac{\delta(\tau)}{\Delta X \Delta Y} & X_0 \leqslant X \leqslant X_0 + \Delta X \qquad Y_0 \leqslant Y \leqslant Y_0 + \Delta Y \\ 0 & \text{otherwise} \end{cases} \qquad (20)$$

Consequently, we substitute the energy generation function $S(X, Y, \tau)$ into the solution Eq. (18) and integrate with respect to time, ζ, over the $0 \leqslant \zeta \leqslant \tau$ domain. Since the source term S is zero within the medium except for the regions $X_0 \leqslant X \leqslant X_0 + \Delta X$ and $Y_0 \leqslant Y \leqslant Y_0 + \Delta Y$, X_0 replaces 0, and $X_0 + \Delta X$ replaces A in the integral range for X, while Y_0 replaces 0, and $Y_0 + \Delta Y$ replaces B in the integral range for Y. Then, by performing the indicated operations, we obtain

$$\theta(X, Y, \tau) = \int_{\xi = X_0}^{X_0 + \Delta X} \int_{\eta = Y_0}^{Y_0 + \Delta Y} \frac{e^{-\tau}}{\Delta X \Delta Y} \sum_{m=0}^{\infty} \sum_{n=0}^{\infty} \frac{\Phi_{mn}(\xi, \eta) \Phi_{mn}(X, Y)}{(\Phi_{mn}, \Phi_{mn})}$$

$$\times \left(\frac{\sin\left(\tau\sqrt{\lambda_{mn} - 1}\right)}{\sqrt{\lambda_{mn} - 1}} + \cos\left(\tau\sqrt{\lambda_{mn} - 1}\right) \right) d\eta \, d\xi \qquad (21)$$

Once the temperature distribution is known, the corresponding heat flux can be determined by applying the general flux law, Eq. (4), to a two-dimensional body described by rectangular coordinates, and expressing the results in dimensionless form as

$$\frac{\partial Q_X(X, Y, \tau)}{\partial \tau} + Q_X(X, Y, \tau) = -\frac{\partial \theta(X, Y, \tau)}{\partial X} \qquad (22a)$$

$$\frac{\partial Q_Y(X, Y, \tau)}{\partial \tau} + Q_Y(X, Y, \tau) = -\frac{\partial \theta(X, Y, \tau)}{\partial Y} \qquad (22b)$$

where the subscripts X and Y in Q represent the direction of heat flow in X and Y, respectively. We then individually integrate Eqs. (22 a) and (22 b) with respect to τ to obtain

$$Q_X(X, Y, \tau) = -e^{-2\tau} \int_{\overline{\tau}=0}^{\tau} e^{2\overline{\tau}} \frac{\partial \theta(X, Y, \overline{\tau})}{\partial X}\, d\overline{\tau} \qquad (22\,c)$$

$$Q_Y(X, Y, \tau) = -e^{-2\tau} \int_{\overline{\tau}=0}^{\tau} e^{2\overline{\tau}} \frac{\partial \theta(X, Y, \overline{\tau})}{\partial Y}\, d\overline{\tau} \qquad (22\,d)$$

If the boundary conditions at four interior surfaces are known, we can introduce the temperature function Eq. (21), into the heat flux relationship given by Eqs. (22 c) and (22 d) to obtain an explicit description of the dimensionless heat flux. For this reason, we now discuss the influence of the boundary conditions on the temperature and heat flux distribution.

For different kinds of boundary conditions the parameters, Φ_{mn} and λ_{mn}, in the temperature solution, Eq. (21), exhibit different values. As mentioned previously, we apply multiple finite sine and cosine transformations to variables X and Y, respectively, for constant wall temperature and adiabatic conditions. Consequently, the dimensionless solution of temperature for constant wall temperature becomes

$$\theta(X, Y, \tau)$$

$$= \frac{2e^{-\tau}}{AB} \left[\sum_{m=1}^{\infty} \sum_{n=1}^{\infty} \frac{\sin(\lambda_m X)\sin(\lambda_n Y)}{\lambda_m \lambda_n} \right.$$

$$\times \frac{\{\cos[\lambda_m(X_0 + \Delta X)] - \cos(\lambda_m X_0)\}\{\cos[\lambda_n(Y_0 + \Delta Y)] - \cos(\lambda_n Y_0)\}}{\Delta X \Delta Y}$$

$$\left. \times \left(\frac{\sin\left(\tau\sqrt{\lambda_{mn} - 1}\right)}{\sqrt{\lambda_{mn} - 1}} + \cos\left(\tau\sqrt{\lambda_{mn} - 1}\right) \right) \right] \qquad (23)$$

As the time τ increases in value, the effects of the boundaries increase, and the temperature function approaches zero because $\theta = 0$ at the four boundaries. The temperature solution in Eq. (23) is substituted into the heat flux relationship, Eqs. (22 c) and (22 d) and the dimensionless heat flux Q_X and Q_Y can been directly obtained.

The temperature distribution for the adiabatic boundary condition is

$$\theta(X, Y, \tau) = \frac{1}{2\,AB}$$

$$+ \frac{e^{-\tau}}{AB} \left[\sum_{m=1}^{\infty} \frac{\cos(\lambda_m X)}{\lambda_m} \frac{\{\sin[\lambda_m(X_0 + \Delta X)] - \sin(\lambda_m X_0)\}}{\Delta X} \right. \qquad (24)$$

$$\times \left(\frac{\sin\left(\tau\sqrt{\lambda_{m0} - 1}\right)}{\sqrt{\lambda_{m0} - 1}} + \cos\left(\tau\sqrt{\lambda_{m0} - 1}\right) \right)$$

$$+ \sum_{n=1}^{\infty} \frac{\cos(\lambda_n Y)}{\lambda_n} \frac{\{\sin[\lambda_n(Y_0 + \Delta Y)] - \sin(\lambda_n Y_0)\}}{\Delta Y}$$

$$\times \left(\frac{\sin\left(\tau\sqrt{\lambda_{0n} - 1}\right)}{\sqrt{\lambda_{0n} - 1}} + \cos\left(\tau\sqrt{\lambda_{0n} - 1}\right) \right)$$

$$+ 2 \sum_{m=1}^{\infty} \sum_{n=1}^{\infty} \frac{\cos(\lambda_m X)\cos(\lambda_n Y)}{\lambda_m \lambda_n} \qquad (24)$$

(Cont.)

$$\times \frac{\{\sin[\lambda_m(X_0 + \Delta X)] - \sin(\lambda_m X_0)\}}{\times \{\sin[\lambda_n(Y_0 + \Delta Y)] - \sin(\lambda_n Y_0)\}}{\Delta X \Delta Y}$$

$$\times \left(\frac{\sin\left(\tau\sqrt{\lambda_{mn} - 1}\right)}{\sqrt{\lambda_{mn} - 1}} + \cos\left(\tau\sqrt{\lambda_{mn} - 1}\right) \right) \Bigg]$$

We note that λ_{00} is a nonzero value resulting in the operator Φ_{00} becoming a constant. This value of λ_{00} for temperature in Eq. (21) must be included in the series and reduces to the first term on the right-hand side of Eq. (24), which represents the steady state portion of the solution. Since any energy released within the insulated region cannot escape, a residual temperature will be evenly distributed over the entire medium, given sufficient time. A comparison of the solutions for different boundary conditions shows that the summation terms for the temperature and heat flux are quite similar. These summations in Eqs. (23) and (24) contain the factor $\exp(-\tau)$. For "large" values of dimensionless time, this exponential factor causes the summations in these equations to approach zero in value. That is, θ, Q_X, and Q_Y go to 0, given conditions of constant wall temperature, and θ goes to $1/(2AB)$ and Q_X, Q_Y go to 0, given adiabatic conditions as time passes.

It is interesting to examine whether the above solutions for the four boundaries insulated in a rectangular plate can be made to approximate those for the one-dimensional problem by assuming the width of a disturbance source along the Y axis is equal to the length of the plate; i.e., $\Delta Y = B$. This problem is similar to the one-dimensional one solved by Özisik and Vick [20], wherein they gave the solutions for considering only a pulsed energy source released adjacent to the insulated boundary surface at $X = 0$. This means the source position was fixed. Therefore, using their results [20], we rewrite temperature and heat flux solutions

for an arbitrarily positioned source as follows:

$$\theta(X, Y, \tau) = \frac{1}{2A} + \frac{e^{-\tau}}{A} \sum_{m=1}^{\infty} \frac{\cos(\lambda_m X)}{\lambda_m} \frac{\{\sin[\lambda_m(X_0 + \Delta X)] - \sin(\lambda_m X_0)\}}{\Delta X}$$

$$\times \left(\frac{\sin\left(\tau\sqrt{\lambda_{m0} - 1}\right)}{\sqrt{\lambda_{m0} - 1}} + \cos\left(\tau\sqrt{\lambda_{m0} - 1}\right) \right) \qquad (25)$$

$$Q_X(X, Y, \tau) = \frac{e^{-\tau}}{A} \sum_{m=1}^{\infty} \sin(\lambda_m X)$$

$$\times \frac{\{\sin[\lambda_m(X_0 + \Delta X)] - \sin(\lambda_m X_0)\}}{\Delta X} \frac{\sin\left(\tau\sqrt{\lambda_{m0} - 1}\right)}{\sqrt{\lambda_{m0} - 1}} \qquad (26)$$

Before presenting representative results, we again examine some interesting limiting cases. First, we consider a limit on the disturbance energy source becoming infinitely concentrated by making the region of an active disturbance source approximate a point; this is $\Delta X \Delta Y \to 0$. Then solutions are found for Eqs. (23) and (24). Alternatively, since the energy source released at time $\tau = 0$ at location $(X, Y) = (X_0, Y_0)$ corresponding to the source term in Eq. (20) can be given by

$$S(X, Y, \tau) = \delta(X - X_0)\delta(Y - Y_0)\delta(\tau) \qquad (27)$$

the solutions for this limiting case can be determined by substituting Eq. (27) into the general solution, Eq. (18). Then the solutions can also be obtained for the following.

Constant wall temperature

$$\theta(X, Y, \tau) = \frac{2e^{-\tau}}{AB} \left[\sum_{m=1}^{\infty} \sum_{n=1}^{\infty} \sin(\lambda_m X)\sin(\lambda_n Y)\sin(\lambda_m X_0)\sin(\lambda_n Y_0) \right.$$

$$\left. \times \left(\frac{\sin\left(\tau\sqrt{\lambda_{mn} - 1}\right)}{\sqrt{\lambda_{mn} - 1}} + \cos\left(\tau\sqrt{\lambda_{mn} - 1}\right) \right) \right] \qquad (28)$$

Adiabatic

$$\theta(X, Y, \tau)$$

$$= \frac{1}{2AB} + \frac{e^{-\tau}}{AB} \left[\sum_{m=1}^{\infty} \cos(\lambda_m X)\cos(\lambda_m X_0) \right.$$

$$\left. \times \left(\frac{\sin\left(\tau\sqrt{\lambda_{m0} - 1}\right)}{\sqrt{\lambda_{m0} - 1}} + \cos\left(\tau\sqrt{\lambda_{m0} - 1}\right) \right) + \sum_{n=1}^{\infty} \cos(\lambda_n Y)\cos(\lambda_n Y_0) \right. \qquad (29)$$

$$\times \left(\frac{\sin\left(\tau\sqrt{\lambda_{0n} - 1}\right)}{\sqrt{\lambda_{0n} - 1}} + \cos\left(\tau\sqrt{\lambda_{0n} - 1}\right)\right)$$

$$+2 \sum_{m=1}^{\infty} \sum_{n=1}^{\infty} \cos(\lambda_m X) \cos(\lambda_n Y) \cos(\lambda_m X_0) \sin(\lambda_n Y_0)$$

$$\times \left. \left(\frac{\sin\left(\tau\sqrt{\lambda_{mn} - 1}\right)}{\sqrt{\lambda_{mn} - 1}} + \cos\left(\tau\sqrt{\lambda_{mn} - 1}\right)\right) \right] \qquad \begin{matrix} (29) \\ (Cont.) \end{matrix}$$

Another interesting limiting case is one in which the finite region is made to approach infinite size by making the limits on $A \rightarrow \infty$ and on $B \rightarrow \infty$. These limiting results can be obtained from Eqs. (23) and (24) and expressed as follows.

Constant wall temperature

$$\theta(X, Y, \tau)$$

$$= \frac{2e^{-\tau}}{\pi^2} \int_{\omega_1=0}^{\infty} \int_{\omega_2=0}^{\infty} \frac{\sin(\omega_1 X) \sin(\omega_2 Y)}{\omega_1 \omega_2}$$

$$\times \frac{\{\cos[\omega_1(X_0 + \Delta X)] - \cos(\omega_1 X_0)\}\{\cos[\omega_2(Y_0 + \Delta Y)] - \cos(\omega_2 Y_0)\}}{\Delta X \Delta Y}$$

$$\times \frac{\sin\left(\tau\sqrt{\omega_1^2 + \omega_2^2 - 1}\right)}{\sqrt{\omega_1^2 + \omega_2^2 - 1}} + \cos\left(\tau\sqrt{\omega_1^2 + \omega_2^2 - 1}\right) d\omega_2 \, d\omega_1 \qquad (30)$$

Adiabatic

$$\theta(X, Y, \tau)$$

$$= \frac{2e^{-\tau}}{\pi^2} \int_{\omega_1=0}^{\infty} \int_{\omega_2=0}^{\infty} \frac{\cos(\omega_1 X) \cos(\omega_2 Y)}{\omega_1 \omega_2}$$

$$\times \frac{\{\sin[\omega_1(X_0 + \Delta X)] - \sin(\omega_1 X_0)\}\{\sin[\omega_2(Y_0 + \Delta Y)] - \sin(\omega_2 Y_0)\}}{\Delta X \Delta Y}$$

$$\times \frac{\sin\left(\tau\sqrt{\omega_1^2 + \omega_2^2 - 1}\right)}{\sqrt{\omega_1^2 + \omega_2^2 - 1}} + \cos\left(\tau\sqrt{\omega_1^2 + \omega_2^2 - 1}\right) d\omega_2 \, d\omega_1 \qquad (31)$$

The limiting solutions for Eqs. (30) and (31) should predict the same temperature and heat flux distributions as given in the solutions for Eqs. (23) and (24), respectively, for times prior to when the thermal wave front is reflected from the described boundaries around the medium, since energy propagates as a wave and

exhibits a distinct wave front with a finite propagation velocity. The physical significance of the foregoing results is examined below.

RESULTS AND DISCUSSION

Numerical computations were performed in order to observe the behavior of a thermal wave induced by an instantaneous thermal disturbance in a two-dimensional plane. Specifically, a disturbance energy source of area $\Delta X \Delta Y$ and concentration $1/\Delta X \Delta Y$, located in the center of the medium, or adjacent to a boundary, or in a corner of the plane was studied to determine the effects of boundary conditions on internal heat transfer. Constant wall temperature and adiabatic conditions at four exterior surfaces that influence the propagation and reflection of thermal waves are discussed in the following results. Equations (23) and (24) are used to compute the temperature and heat flux for constant wall temperature and adiabatic boundary conditions, respectively. The temperatures predicted by the one- and two-dimensional analyses are compared in order to emphasize the significant differences between the two formulations. An examination of the series solutions shows that the exponential term written as $\exp(-\tau)$ is independent of m and n and does not contribute to convergence of the solutions. Therefore Eqs. (23) and (24), in particular, are expected to converge slowly. As is generally known, the Green's function for hyperbolic conduction converges more slowly than that for parabolic conduction, and the solutions for the wave front also converge more slowly than those for other situations. Furthermore, the accuracy and convergence of the series analytical solution were both verified using the numerical method developed by Yang [18], which resolves the multidimensional thermal waves without introducing oscillation or dissipation.

Figure 2 shows three-dimensional sketches of dimensionless temperature at different dimensionless times for adiabatic boundary conditions and an instantaneous thermal disturbance located in the center of the medium. Additional temperature profiles at fixed position $Y = 0.5$ are displayed in Figure 3, in order to understand the propagation and reflection of the thermal wave more clearly. The boundary around the plate is insulated, preventing heat from being transferred through the boundaries and reflecting the energy back completely. The initial dimensionless temperature is 0. Clearly, when the thermal disturbance occurred at the center over the region $\Delta X \Delta Y = 0.01$ at $\tau = 0^+$ and the temperature suddenly increased to 100, an annular thermal wave was generated and propagated in all directions at a constant speed of 1. Note that all energy was concentrated in a wave front of finite width, which was preserved during all reflection-transmission effects. The front width was equal to ΔX or ΔY, but an entire front had not yet formed prior to $\tau < 0.1$. The amplitude of the annular wave front has its highest value along the direction normal to the boundary because the energy source is assumed to be square. In other words, if the directions of a traveling front deflect from the X and Y axes, then the energy of a front would be dissipated more rapidly than that along X and Y axial to induce a lower concentration due to a sudden increase in the energy diffusible region. The striking feature in these results, which is different from that of the one-dimensional analysis presented by Vick and Özisik [16], is the negative trailer generated and forming a minus-amplitude peak in the
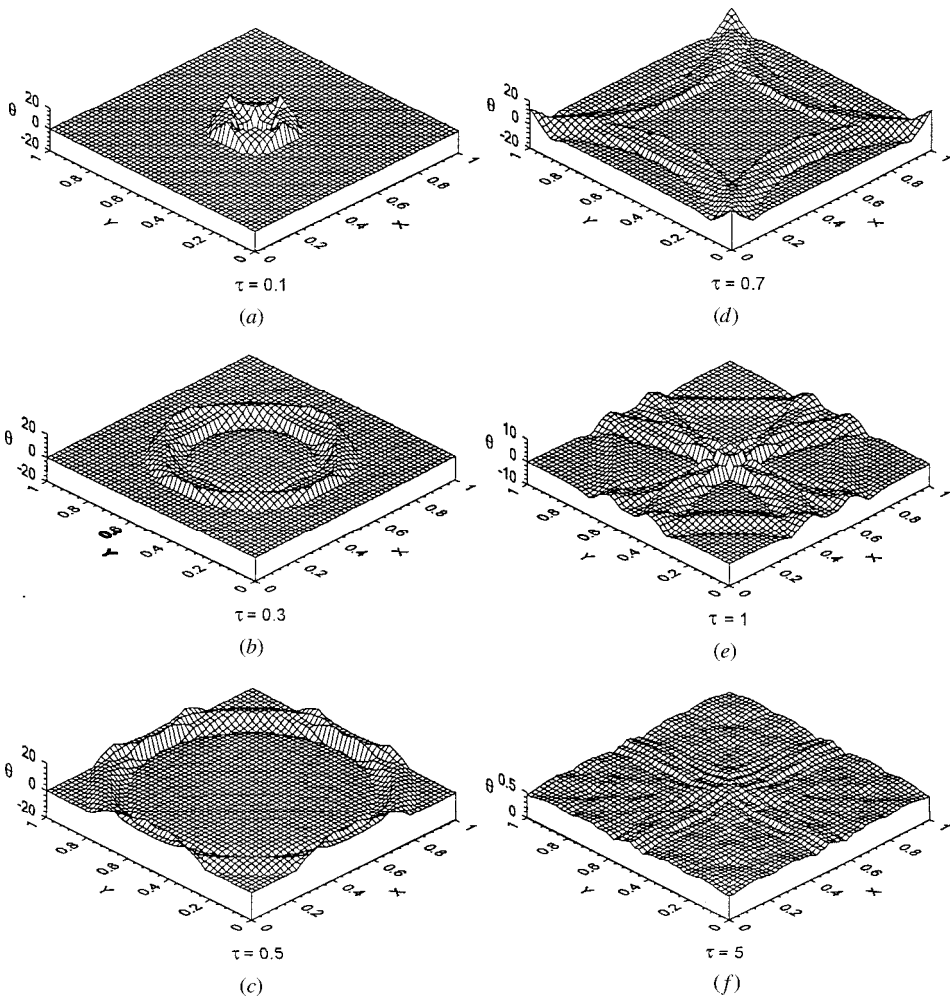
Figure 2. Three-dimensional temperature sketch at different times for adiabatic boundary conditions for an instantaneous thermal disturbance located in the center of the medium.

vicinity of origin of the heat source when $\tau > 0.05$. The minus peak follows after the wave front until diffusion phenomena become dominant and is of the same order of magnitude as the wave front peak. Another phenomenon of particular interest is the wave front being attenuated to a sharp front and the presence of a tip at the fore that differs from the uniform front displayed in the one-dimensional analysis. These phenomena are discussed in conjunction with Figure 8.

As time passes, the positive thermal wave accompanies a negative trailer to propagate toward the boundary, and the two wave cusps decay exponentially while dissipating their energy along their path and diffusing it over a more extensive region. Also, since the external boundaries are insulated for all $\tau > 0$, the total energy content is constant, so that the heat flux normal to the walls is zero, as
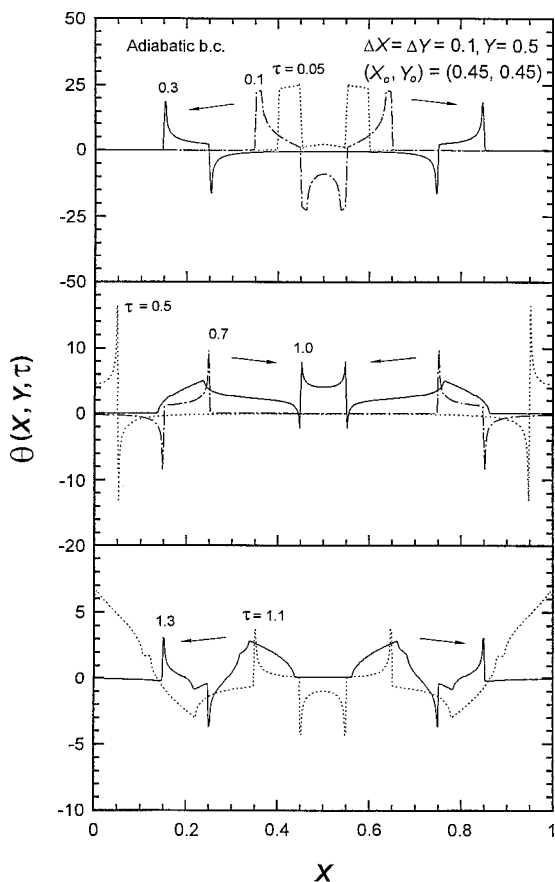
Figure 3. Temperature profiles at $Y = 0.5$ corresponding to the situations described in Figure 2.

shown in Figure 4. As the wave propagates forward, energy is deposited in its wake by diffusion and induces a small negative residual temperature due to the effect of the negative wave. At $\tau = 0.45$ the leading edge of the wave front contacts the exterior insulated surfaces and starts being reflected, and at $\tau = 0.5$ the half crest of the wave has fully encountered these surfaces at $X = 0.5$ and $Y = 0.5$, as shown in Figure 3. Thus the hyperbolic heat conduction equation predicts that a thermal wave disturbance tends to propagate in a given direction until its course is impeded by a barrier. When $\tau = 0.7$, the four wave fronts generated by the four adiabatic boundaries exhibit positive amplitudes and are accompanied by negative waves, as previously seen. Figure 2 d shows that the thermal waves move directly back toward the origin. These fronts then begin to cross each other and are strengthened due to combination in the regions of intersection, as is clearly seen at the corners. In addition, extra waves generated by the four corners have traveled a considerable distance at $\tau = 1.0$, as shown in Figure 2 e. At this moment the four waves reflected by the boundaries arrive simultaneously at the center of the plane. This transmis-
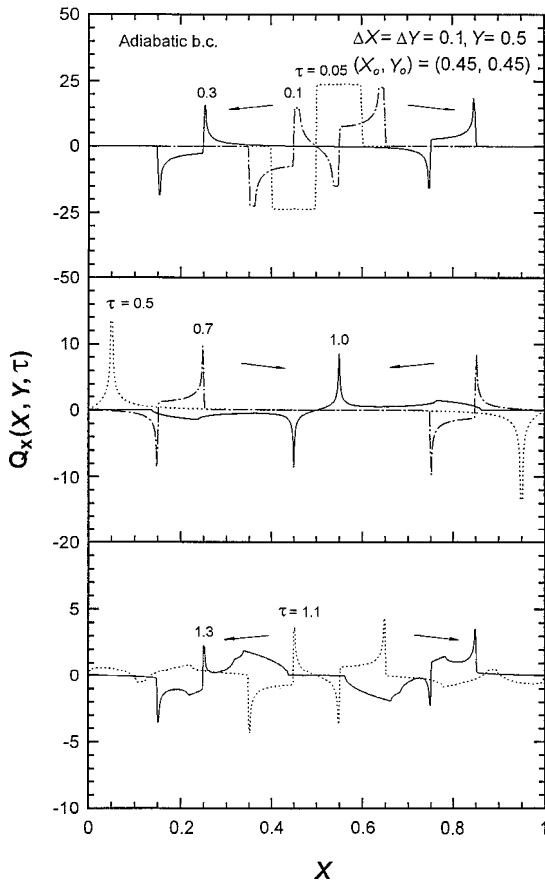
Figure 4. Heat flux profiles in the X direction at $Y = 0.5$ corresponding to the situations described in Figure 2.

sion-reflection-combination phenomenon persists until diffusion dominates. As more time passes, the temperature distribution becomes smoother and more uniform, until the residual temperature approximates its ultimate constant, as shown at $\tau = 5.0$.

Figure 4 shows the heat flux Q_X profiles at $Y = 0.5$ corresponding to the conditions shown in Figure 2. Again a severe thermal wave front with a reverse trailer can be observed where the heat flux displays antisymmetry at the heat source center, since the propagation directions of the thermal wave are opposite in Figure 4. That is, if the positive wave front is moving in the negative X direction, the corresponding magnitude of the heat flux in the wave front and in the wake of the front is opposite to that moving in the positive X direction. After the front is reflected by boundaries, the wave front is converted into an inverse wave front and moves toward the center of the plane. In addition, in this configuration with the heat flux in the Y direction, Q_Y is always equal to zero due to symmetry, which means the energy does not cross the surface of $Y = 0.5$ and is equivalent to the

adiabatic condition. When $\tau = 1.0$, the temperature profile in Figure 3 shows evidence of three obvious thermal waves, but in practice, the two wider waves and part of the main wave come from reflections off the boundaries $Y = 0$ and 1. Therefore the Q_Y of the two wider waves are lower than θ in Figure 3. Moreover, the depressions between the three waves are induced by the accompanying negative trailer reflected by the adiabatic surfaces at $X = 0$ and 1.

Figure 5 shows the temperature distributions of the whole domain at various times (i.e., $\tau = 0.1, 0.3, 0.5, 0.7, 1.0, 5.0$) for which the physical assumptions are the same as those in Figure 2, except that the boundary conditions are maintained at $\theta = 0$ so that heat can be absorbed rapidly by the environment. Figures 6 and 7 display the temperature and heat flux profiles, respectively, at $Y = 0.5$ for different
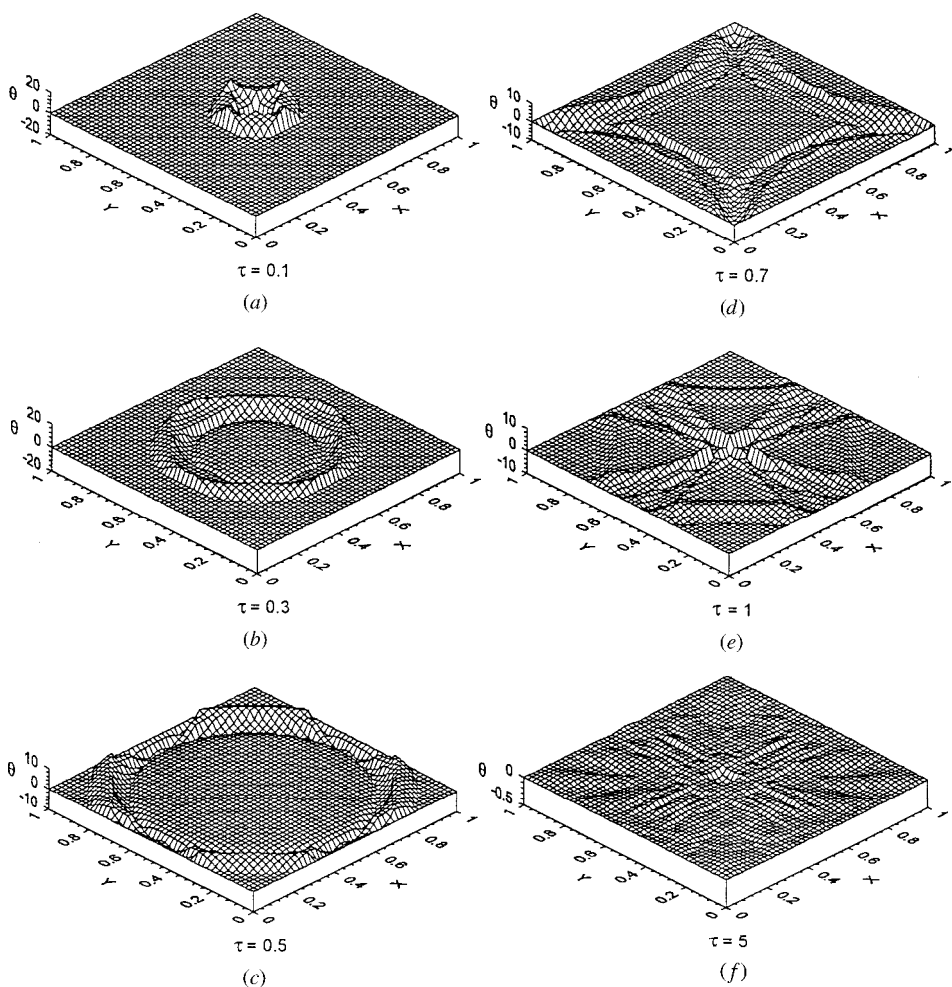

Figure 5. Three-dimensional temperature sketch at different times for conditions of constant wall temperature boundary for an instantaneous disturbance located in the center of the medium.
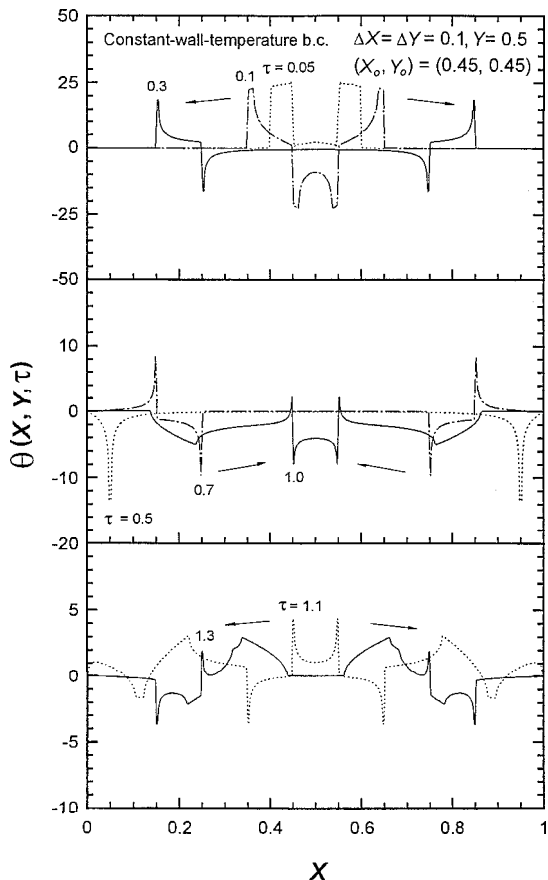
Figure 6. Temperature profiles at $Y = 0.5$ corresponding to the situations described in Figure 5.

times. At any time before the wave encounters the boundaries ($\tau < 0.45$), the behavior of the thermal wave and the temperature and heat flux profile coincide with that of the case shown in Figures 2–4. When $\tau = 0.1$, the temperature profile is identical to the graph in Figure 2a, since the wave front is unaffected by the boundary effect at this time. The reflected portion, which initially encounters the boundaries at $\tau = 0.45$ and starts being reflected, shows a negative thermal wave with a positive trailer moving toward the origin at $\tau = 0.7$. This negative wave front results from the enhanced ability of an environment to transmit energy and the basic criterion for energy conservation. Conversely, the negative trailer behind the incident front is transformed into a positive one by reflection because the capacity for heat transfer from the environment to the medium is correspondingly strengthened. The internal reflections are produced at the interface between two dissimilar media in a two-region slab exposed to a pulsed volumetric source. The reflected waves in region 1 may be positive or negative in magnitude as determined by the thermal conductivity in region 2. The effects of region 2 are similar to those of the
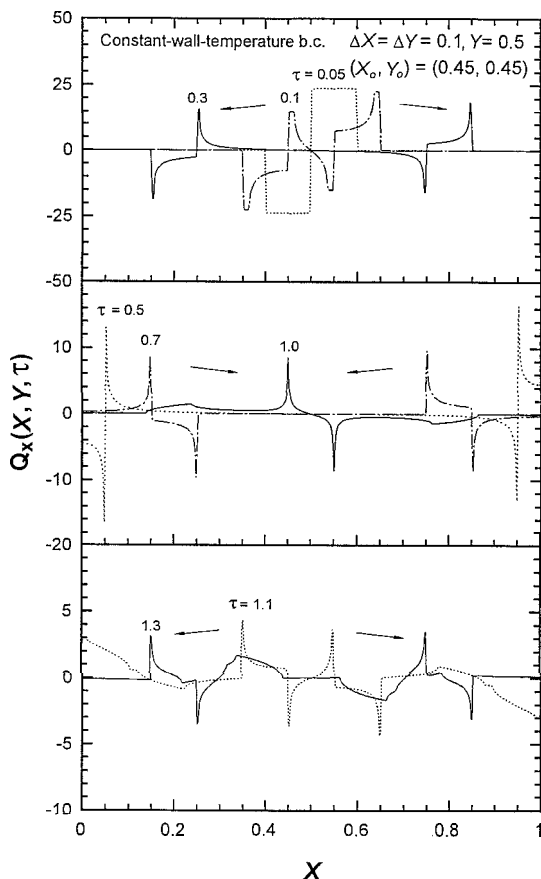
Figure 7. Heat flux profiles in the X direction at $Y = 0.5$ corresponding to the situations described in Figure 5.

environment in our cases. The positive reflected wave resulting from adiabatic boundary conditions in our studies can be simulated by assuming the thermal conductivity of region 1 to be lower than that of region 2, as in their study [28]. In contrast, the negative reflected wave due to the boundary at $\theta = 0$ can be simulated by assuming the thermal conductivity of region 1 to be higher than that of region 2. Figures 5e–5f display the complicated temperature profile in the plane due to boundary reflections and wave interactions. As time passes, the effect of the wave gradually decreases until the temperature profile is uniform and approaches zero.

   To clarify the causes for a negative trailer formed after the wave front, the different lengths of disturbance sources along the Y axis, i.e., $\Delta Y = 1$, 0.5, and 0.05, but the same $\Delta X = 0.1$ are compared in Figure 8, and the case in which $\Delta X = \Delta Y = 0.1$, in Figure 3, must also be compared. The temperature profiles at $Y = 0.5$ are shown in Figure 8 for three times, $\tau = 0.05$, 0.1, and 0.3. In general, decreasing the disturbance area causes the energy concentration in the wave front to increase,
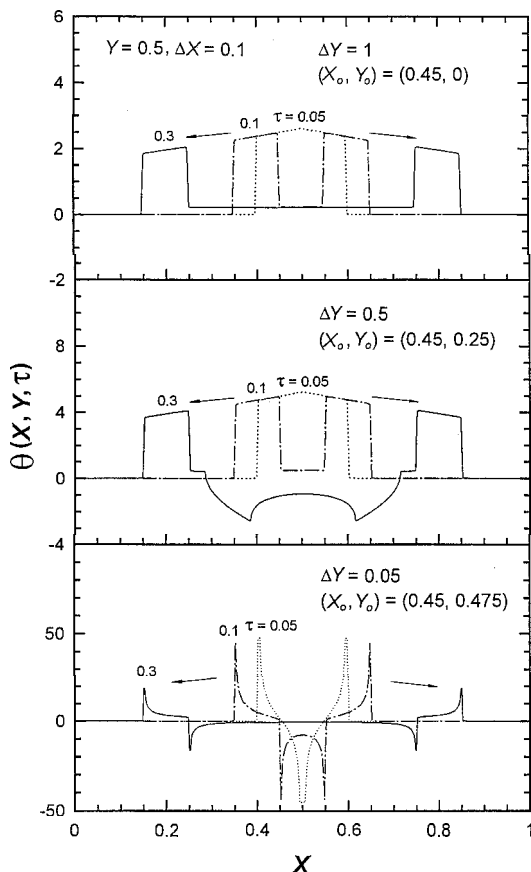
Figure 8. Comparison of temperature distributions for the different lengths of disturbance sources along Y axis, $\Delta Y = 1$, 0.1, and 0.05, all at the same $\Delta X = 1$.

with the peak becoming more severe for the same energy content. If we were to continue at the limit as the disturbance concentration became infinite over an infinitesimally small disturbance region, the limiting delta function behavior described by solutions Eqs. (28) and (29) for the case in which $\Delta X \Delta Y \to 0$ would be obtained. The other evident phenomenon is that as ΔY decreases, the negative trailer occurs earlier and is more concentrated. This phenomenon was not found in any previous studies of thermal waves. A negative temperature means the temperature is below the initial temperature. $\Delta Y = 1$ with adiabatic boundary conditions around the rectangular plane can be reduced to the one-dimensional heat conduction model in which no negative trailer is generated, since the directions of heat transfer are restricted to one direction. Whereas, as ΔY decreases from 1, the temperature distribution at the center of the plane will be exposed to the stronger

influence of Y direction heat conduction. In other words, the disturbance source is far removed from the insulated boundaries, which will involve the undisturbed regions in absorbing the released energy. Therefore, in order for the thermal wave to move in more directions and keep its wave nature; i.e., possession of an energy-concentrated thermal wave front, the negative-temperature trailer is gener-ated to preserve the energy content of the system. According to the above results, we find that the negative trailer occurs only when the reflected portion from a pair of opposite insulated surfaces arrives at the center of the disturbance location and strengthens the temperature magnitude. If the disturbance region persists in decreasing, a negative trailer is generated earlier and easier. In addition, for small-disturbance regions the peak of the negative trailer is lower in magnitude and closer to the wave front at the same moment than that for large-disturbance regions. At a time equal to one-half the front width ($\tau = \Delta X = 0.05$), the tempera-ture profiles for $\Delta Y = 1$ and 0.5 at $Y = 0.5$ are exactly the same, and the front has not yet separated into two portions traveling in opposite positive and negative X directions, whereas for $\Delta Y = 0.1$ the fronts heading in different directions have formed at this time but the negative trailers have not yet appeared. On the other hand, when $\Delta Y = 0.05$, the trailer has induced a severe front. In the center of Figure 8 and the upper portion of Figure 3, we can clearly see the beginning of the negative trailer. When the trapezoidal wave front starts to move toward the boundaries, the two sides of the wave front decrease in magnitude exponentially until they reach the negative trailer adjacent to the edge of the front. Once the trailer meets the trapezoidal wave front, it starts to attenuate to the front rapidly in amplitude until only a severe tip is left at the leading edge. The process of trailer production is more difficult to observe as the region of thermal disturbance becomes smaller.

CONCLUSIONS

The transient temperature distribution and heat flux in a two-dimensional rectangular plate with a thermal disturbance instantaneously released over a finite area have been determined using the hyperbolic heat conduction model. All surfaces around the plate were assumed to be at either a constant wall temperature or an adiabatic condition. The thermophysical properties were also assumed to be constant, so that analytic solutions to the problem could be obtained by using the Green's function technique. The results of the present analysis, showing the contour of a thermal wave generated by a thermal disturbance possessing a concentrated thermal wave front with an accompanying negative trailer, are significantly different from those obtained through one-dimensional analysis. The formation of a negative trailer and a sharp peak existing at the leading edge of the front, which decay exponentially along its path of travel because of dissipating energy in its wake, result from an increase in the diffusible region as it travels through the medium. Because of overlapping and interaction of the reflected wave fronts and trailers from the peripheral surfaces, the sharp peaks of the thermal wave are more complicated than those found through one-dimensional analysis. Furthermore, a comparison of temperature distributions derived from the hyper-

bolic and parabolic models reveals that the parabolic model significantly underestimates temperatures in the beginning, as the wave phenomenon is obvious.

REFERENCES

1. V. Peshkov, Second Sound in Helium II, *J. Phys. USSR*, vol. 8, p. 381, 1994.
2. R. J. Von Gutfeld, Heat Pulse Transmission, in W. P. Masoned (ed.) *Physical Acoustics: Principles and Methods*, vol. 5, p. 233, Academic Press, New York, 1968.
3. M. J. Maurer and H. A. Thompson, Non-Fourier Effects at High Heat Flux, *ASME J. Heat Transfer*, vol. 95, pp. 284–286, 1973.
4. D. D. Joseph and L. Preziosi, Heat Waves, *Rev. Mod. Phys.*, vol. 61, pp. 41–73, 1989.
5. D. D. Joseph and L. Preziosi, Addendum to the Paper on Heat Waves, *Rev. Mod. Phys.*, vol. 62, pp. 375–391, 1990.
6. C. Cattaneo, A Form of Heat Conduction Equation which Eliminates the Paradox of Instantaneous Propagation, *Compte Rendus*, vol. 247, pp. 431–433, 1958.
7. P. Vernotte, Les Paradoxes de la Theorie Continue de l'Equation de la Chaleur, *Compte Rendus*, vol. 246, pp. 3154–3155, 1958.
8. R. E. Nettleton, Relaxation Theory of Thermal Conduction in Liquids, *Phys. Fluids*, vol. 3, pp. 216–225, 1960.
9. H. P. Francis, Thermo-Mechanical Effects in Elastic Wave Propagation: A Survey, *J. Sound Vibration*, vol. 21, pp. 181–192, 1972.
10. S. Sieniutycz, The Variational Principles of Classical Type for Non-Coupled Nonstationary Irreversible Transport Processes with Convective Motion and Relaxation, *Int. J. Heat Mass Transfer*, vol. 20, pp. 1221–1231, 1977.
11. W. Kaminski, Hyperbolic Heat Conduction Equation for Materials with a Nonhomogeneous Inner Structure, *ASME J. Heat Transfer*, vol. 112, pp. 555–560, 1990.
12. K. Mitra, S. Kumar, A. Vedavarz, and M. K. Moallemi, Experimental Evidence of Hyperbolic Heat Conduction in Processed Meat, *ASME J. Heat Transfer*, vol. 117, pp. 568–573, 1995.
13. M. N. Özisik and D. Y. Tzou, On the Wave Theory in Heat Conduction, *ASME J. Heat Transfer*, vol. 116, pp. 526–535, 1994.
14. D. Y. Tzou, On the Thermal Shock Wave Induced by a Moving Heat Source, *ASME J. Heat Transfer*, vol. 111, pp. 232–238, 1989.
15. K. J. Baumeister and T. D. Hamill, Hyperbolic Heat Conduction Equation: A Solution for the Semi-Infinite Body Problem, *ASME J. Heat Transfer*, vol. 91, pp. 543–548, 1969.
16. B. Vick and M. N. Özisik, Growth and Decay of a Thermal Pulse Predicted by the Hyperbolic Heat Conduction Equation, *ASME J. Heat Transfer*, vol. 105, pp. 902–907, 1983.
17. H. Q. Yang, Characteristics-Based, High-Order Accurate and Nonoscillatory Numerical Method for Hyperbolic Heat Conduction, *Numer. Heat Transfer Part B*, vol. 18, pp. 221–241, 1990.
18. H. Q. Yang, Solution of Two-Dimensional Hyperbolic Heat Conduction by High-Resolution Numerical Methods, *Numer. Heat Transfer Part A*, vol. 21, pp. 339–349, 1992.
19. H. T. Chen and J. Y. Lin, Numerical Analysis for Hyperbolic Heat Conduction, *Int. J. Heat Mass Transfer*, vol. 36, pp. 2891–2898, 1993.
20. M. N. Özisik and B. Vick, Propagation and Reflection of Thermal Waves in a Finite Medium, *Int. J. Heat Mass Transfer*, vol. 27, pp. 1845–1854, 1984.
21. A. Haji-Sheikh and J. V. Beck, Green's Function Solution for Thermal Wave Equation in Finite Bodies, *Int. J. Heat Mass Transfer*, vol. 37, pp. 2615–2626, 1994.

22. J. P. Wu, Y. P. Shu, and H. S. Chu, Transient Heat Transfer Phenomenon of Two-Dimensional Hyperbolic Heat Conduction Problem, *Numer. Heat Transfer Part A*, vol. 33, pp. 635–652, 1998.

23. K. K. Tamma and R. R. Namburu, Computational Approaches with Applications to Nonclassical and Classical Thermomechanical Problems, *Appl. Mech. Rev.*, vol. 50, pp. 514–551, 1997.

24. K. K. Tamma and X. Zhou, Macroscale and Microscale Thermal Transport and Thermomechanical Interactions: Some Noteworthy Perspectives, *J. Thermal Stress*, vol. 21, pp. 405–449, 1998.

25. P. M. Morse and H. Feshback, *Methods of Theoretical Physics*, Part I, pp. 865–869, McGraw-Hill, New York, 1953.

26. I. N. Sneddon, *Fourier Transforms*, pp. 71–82, McGraw-Hill, New York, 1951.

27. M. I. Flik and C. L. Tien, Intrinsic Thermal Stability of Anisotropic Thin-Film Superconductors, *ASME J. Heat Transfer*, vol. 112, pp. 10–15, 1990.

28. J. I. Frankel, B. Vick, and M. N. Özisik, General formulation and analysis of hyperbolic heat conduction in composite media, *Int. J. Heat Mass Transfer*, vol. 30, pp. 1293–1305, 1987.